Global minima for transition metal clusters described by Sutton–Chen potentials

Jonathan P. K. Doye[a] and David J. Wales*[,b]

[a] *FOM Institute of Atomic and Molecular Physics, Kruislaan 407, 1098 SJ Amsterdam, The Netherlands*
[b] *University Chemical Laboratory, Lensfield Road, Cambridge, UK CB2 1EW*

Using a Monte Carlo minimization approach we report the global minima for metal clusters modelled by the Sutton–Chen family of potentials containing up to 80 atoms. The resulting structures are discussed in the light of both experimental and theoretical data for clusters of the appropriate elements.

The structure is the most fundamental property of a cluster and is important for understanding all aspects of chemical and physical behaviour. Unfortunately, there is, as yet, no direct method for determining the structure of free clusters in molecular beams. Instead, one has to measure properties that depend upon geometry and then try to infer the structure by comparing the results with the predictions of models. This approach has been combined with techniques such as electron diffraction,[1] mass spectral abundances,[2] chemical reactivity,[3] magnetism[4] and X-ray spectroscopy.[5]

For transition metal clusters a wealth of structural information is now becoming available from increasingly sophisticated experiments. One of the most powerful techniques is the flow-reactor approach, which probes the chemical reactivity of size-selected clusters. For example, this method has been applied to nickel clusters using nitrogen as the chemical probe, to give detailed information for all sizes up to 71 atoms.[6–10] From these data it has been possible to make structural assignments around 13 and 55 atoms (sizes of complete Mackay icosahedra[11]). However, in the size range $29 \leqslant N \leqslant 48$ only one structural assignment has so far been made because of the large number of possible geometries to be considered and the presence of multiple isomers.[9]

Hence, it is increasingly important for theory to guide the interpretation of experiment by producing reliable structural models. However, for transition metal clusters this is an extremely demanding task. It is now becoming possible to perform *ab initio* calculations for clusters at the larger end of the size range that we consider here ($N \leqslant 80$)[12,13] but only for a few fixed structures of high symmetry. It is not feasible to perform the extensive search of the potential energy surface required to find the most stable structure. Instead, one has to use empirical potentials. Even with these simplified descriptions of the interatomic interactions it can be a very difficult task to find the global minimum for the size range considered here. However, we are confident that in this work likely candidates for the global minima have been located. Our optimism is based upon the performance of the chosen algorithm in previous studies[14] and the large database of structures we have acquired through work on clusters bound by the Morse potential.[15,16]

Atomic clusters usually adopt one of three morphologies: icosahedral, decahedral or close-packed. Particularly stable examples of each are illustrated in Fig. 1. Icosahedra and decahedra exhibit five-fold axes of symmetry, which is possible in finite systems due to the absence of translational periodicity. The Mackay icosahedron[11] [Fig. 1(*b*)] can be decomposed into 20 face-centred cubic (fcc) tetrahedra sharing a common vertex. Decahedra are based upon pentagonal bipyramids made up of five fcc tetrahedra sharing a common edge. The most stable decahedral form, the Marks decahedron[17] [Fig. 1(*c*)], involves further facetting to make the cluster more spherical whilst keeping the proportion of the surface exhibiting {100} facets to a minimum. The most stable fcc

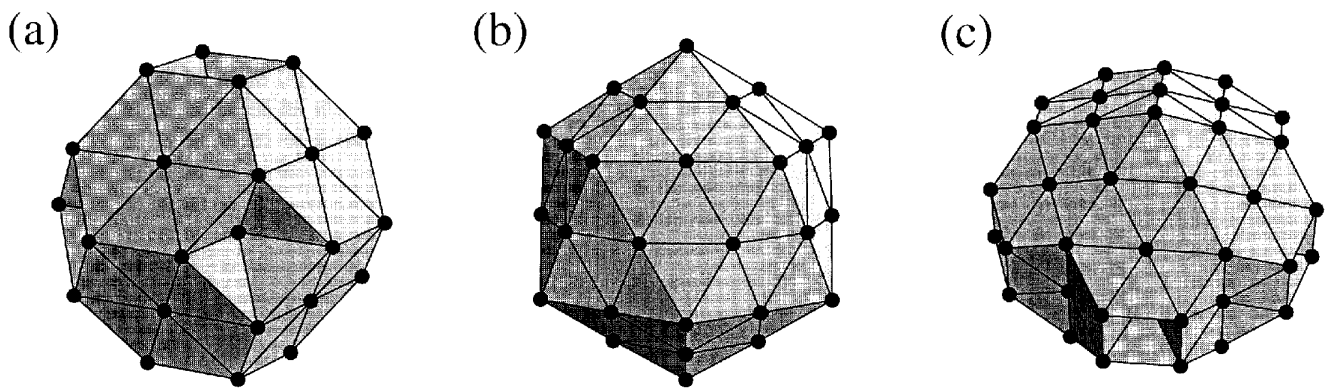

Fig. 1 Example morphologies: (*a*) 38-atom truncated octahedron, (*b*) 55-atom Mackay icosahedron and (*c*) 75-atom Marks decahedron. These clusters have optimal shapes for the three main types of ordered packing seen in this study: face-centered cubic (fcc), icosahedral and decahedral, respectively. The latter two morphologies cannot be extended to the bulk because they possess five-fold axes of symmetry. All three structures are global minima for the SC 12–6 and 9–6 potentials while only the Mackay icosahedron is not the global minimum for the 10–8 potential

cluster is the truncated octahedron. All three morphologies are commonly seen in the metal clusters supported on surfaces.[18]

In this paper we seek to further our understanding of transition metal clusters and aid structural assignments from experimental data by performing global optimization for clusters containing up to 80 atoms described by the Sutton–Chen family of potentials. In the next section we describe the methods used and in the following section we describe the structures of the global minima and compare them to experimental results and previous theoretical studies.

Methods

Potentials

The Sutton–Chen (SC) potential has the form:[19]

$$E = \varepsilon \sum_i \left[\frac{1}{2} \sum_{j \neq i} \left(\frac{a}{r_{ij}} \right)^n - c\sqrt{\rho_i} \right],$$

where

$$\rho_i = \sum_{j \neq i} \left(\frac{a}{r_{ij}} \right)^m.$$

c is a dimensionless parameter, ε is a parameter with dimensions of energy, a is the lattice constant, and m and n are positive integers with $n > m$. We use the n, m and c parameters given by Sutton and Chen[19] for the metals Ag, Ni and Au; Rh has the same scaled parameters as Ag, Cu the same ones as Ni and Pt is the same as Au, so the corresponding results for these metals can be obtained from their partners by rescaling. For Ag and Rh, $n = 12$, $m = 6$ and $c = 144.41$; for Ni and Cu, $n = 9$, $m = 6$ and $c = 39.432$; for Au and Pt, $n = 10$, $m = 8$ and $c = 34.408$. In the present calculations we employed reduced units with $\varepsilon = 1$ and $a = 1$. The tabulated results may therefore easily be rescaled for any of the above elements. The appropriate energy is given by multiplying the reduced energy by ε, whilst the coordinates need to be multiplied by a, the lattice constant.

The Sutton–Chen potential incorporates an approximate many-body representation of the delocalized metallic bonding, but it does not include any directional terms, which are likely to be important for transition metals with partially occupied d shells.[19] Numerous studies, particularly of surfaces and bulk, have now employed SC potentials and we will only mention a few of these here. For platinum (10–8) and rhodium (12–6), the appropriate SC potentials correctly predict the experimental ordering of the direct and exchange surface migration processes.[20] Todd and Lynden-Bell found that surface energies, stresses, relaxation and reconstructions of fcc metals were reasonably well reproduced by SC potentials,[21] while Blumberg *et al.* employed the SC framework to study stress-induced failure in metals.[22] The melting of platinum and the stability limit of the crystalline phase were also investigated along with the surface free energy using order parameter techniques.[23] Hammonds found that SC potentials generally perform better in describing microfacetting reconstructions and step roughening than for contractive surface reconstructions.[24] Lynden-Bell investigated induced disorder, failure and fracture of metals under uniaxial tension using SC potentials and gained new insight into the corresponding mechanisms.[25]

The popularity of SC potentials is partly due to the computationally tractable form adopted for the many-body forces, as well as the reasonable agreement with experiment. It is the relatively simple analytic form of the potential that has enabled us to produce a thorough account of global minima in the present work.

Global optimization methods

The main method we used to find the lowest minima is based upon Li and Scheraga's Monte Carlo minimization[26] or 'basin-hopping' algorithm, which we have recently employed for several systems.[14,16,27] This approach belongs to the family of 'hypersurface deformation' methods[28] where the energy is transformed, usually to a smoother surface with fewer minima. The lowest minimum of the new surface is then mapped back to the original surface, but there is no guarantee that the global minima on the two surfaces are related and often they are not.[15] In contrast, the transformation that we apply is guaranteed to preserve the global minimum. The transformed energy $\tilde{E}$ is defined by $\tilde{E}(\mathbf{X}) = min\{E(\mathbf{X})\}$, where $\mathbf{X}$ represents the vector of nuclear coordinates and *min* signifies that an energy minimization is performed starting from $\mathbf{X}$.

The topography of the transformed surface is that of a multi-dimensional staircase. Each step corresponds to the basin of attraction surrounding a particular minimum, that is the set of geometries where geometry optimization leads to that minimum. The transformation has a significant effect on the dynamics. Not only are transitions to a lower energy minimum barrierless, but they can also occur at any point along the boundary between basins of attraction, whereas on the untransformed surface transitions can occur only when the system passes along the transition state valley. As a result intrawell vibrational motion is removed and the system can hop directly between minima at each step. The success of the basin-hopping method for potential energy surfaces that exhibit multiple funnels has been explained elsewhere in terms of the thermodynamics of the transformed landscape.[27] Similar methods have been used in studies of biomolecules.[29–31]

To explore the $\tilde{E}$ surface we have used canonical Monte Carlo (MC) sampling at reduced temperatures of $T^* = 30$, 5 and 10 for the 12–6, 10–8 and 9–6 potentials, respectively, where the reduced temperature is kT/ε. To restrict the configuration space to bound clusters we reset the coordinates to those of the current minimum in the Markov chain at each step.

In our recent application to Lennard-Jones clusters the MC minimization approach outperformed all other methods in the literature, finding all the known lowest energy Lennard-Jones clusters up to 110 atoms, including those with non-icosahedral global minima.[14] All our published results are available in downloadable form from the Cambridge Cluster Database.[32]

In a recent study we found the global minima of clusters bound by Morse potentials for all sizes up to 80 atoms as a function of the range of the interaction.[15,16] For this potential there are at least 350 different global minima in this size range. Most of the global minima have icosahedral, decahedral or closed-packed structures, and these were mainly found by considering the structures that have the largest number of nearest-neighbour contacts for each morphology.[33] To complement the basin-hopping calculations in the present work we reoptimized all the Morse global minima and low-lying structures for the SC potentials.

Results and Discussion

The energies and point groups of all the global minima are given in Table 1. The basin-hopping algorithm found 95% of the 12–6 global minima, 94% of the 9–6 and 85% of the 10–8. Five runs from different random starting points consisting of 5000 MC steps each were used for each cluster size. These results generally confirm the utility and robustness of the basin-hopping approach. Most of the failures occur when the global minimum has a close-packed geometry that is only marginally lower in energy than an icosahedral or decahedral structure. In such cases the topography of the potential energy surface is likely to have multiple funnels, a scenario that often makes global optimization extremely difficult.[27,34] We have not made any systematic attempt to find the optimal tem-

Table 1 Global minima for Sutton–Chen 12–6, 9–6 and 10–8 clusters with $N \leqslant 80$. For each minimum the energy and point group (PG) are given and a structural assignment (SA) made if possible. The structural categories are: icosahedral with an anti-Mackay (aM) or a Mackay overlayer (M); decahedral with *n* atoms along the decahedral axis (d*n*); close-packed fcc (f), hcp (h), or involving a mixture of stacking sequences and twin planes (c); and clusters involving disclination lines (dis)

	12–6			9–6			10–8		
N	Energy/ε	PG	SA	Energy/ε	PG	SA	Energy/ε	PG	SA
3	−1704.6905	D_{3h}		−480.8560	D_{3h}		−633.7771	D_{3h}	
4	−2601.8447	T_d		−709.5396	T_d		−904.1153	T_d	
5	−3461.3452	D_{3h}		−929.7341	D_{3h}		−1163.7670	D_{3h}	
6	−4378.8875	O_h		−1163.9640	O_h		−1433.8252	O_h	
7	−5271.2947	D_{5h}		−1388.5116	D_{5h}		−1695.8893	D_{5h}	
8	−6129.7564	D_{2d}		−1611.8509	D_{2d}		−1954.1206	D_{2d}	
9	−7048.7552	C_{2v}		−1839.9790	C_{2v}		−2218.1861	C_{2v}	
10	−7972.0971	C_{3v}		−2072.2436	C_{3v}		−2481.7019	C_{3v}	
11	−8889.9627	C_{2v}		−2302.4939	C_{2v}		−2741.5489	C_{2v}	
12	−9871.2458	C_{5v}		−2543.1611	C_{5v}		−3005.9274	C_2	
13	−10 968.5082	I_h	M	−2808.5765	I_h	M	−3280.3843	I_h	M
14	−11 798.8479	C_{3v}	aM	−3023.9716	C_{3v}	aM	−3549.4023	C_{6v}	dis
15	−12 742.9841	C_{2v}	aM	−3267.5300	D_{6d}	dis	−3825.6495	C_{2v}	
16	−13 672.6475	C_s	aM	−3505.2600	C_s		−4101.6928	C_s	
17	−14 606.3231	C_2	aM	−3742.6166	C_{2v}		−4371.8696	C_s	
18	−15 535.3810	C_s	aM	−3978.1268	C_{2v}		−4640.1812	C_s	
19	−16 595.0561	D_{5h}	aM	−4221.3539	D_{5h}	aM	−4906.0562	C_s	
20	−17 510.9209	C_{2v}	aM	−4455.5507	C_{2v}	aM	−5171.2334	C_{2v}	
21	−18 433.0300	C_1	aM	−4700.7823	C_1		−5439.9207	C_{6v}	dis
22	−19 422.7209	C_s		−4949.3235	C_s		−5716.6689	C_s	
23	−20 383.3977	D_{3h}		−5191.4317	C_2		−5990.7388	C_2	
24	−21 315.4208	C_{2v}	h	−5427.4229	C_2		−6266.6622	C_s	
25	−22 339.6319	C_{3v}	d3	−5670.7723	C_3		−6533.1606	C_1	
26	−23 337.2211	D_{3h}	h	−5920.3488	D_{3h}	h	−6803.6959	C_s	
27	−24 284.3891	C_s	h	−6165.3671	C_s		−7080.7248	C_s	
28	−25 276.9501	C_{3v}	M	−6411.2387	C_1		−7354.7939	C_1	
29	−26 263.2779	C_{2v}	d4	−6654.0358	C_2		−7632.7382	C_2	
30	−27 253.8536	C_{2v}	d3	−6903.2657	C_s		−7909.1542	C_{3v}	
31	−28 274.4371	C_{2v}	d4	−7153.4410	C_3		−8171.0816	C_1	
32	−29 265.3320	C_{2v}	M	−7400.8234	D_{2d}		−8451.6848	C_3	
33	−30 274.9603	C_{2v}	d4	−7644.6441	C_s	d4	−8726.4506	C_s	d4
34	−31 231.7697	C_{2v}	c	−7889.3674	C_2		−9005.3502	C_3	
35	−32 280.3945	C_{2v}	d4	−8147.0475	D_3		−9276.2927	C_s	
36	−33 253.9352	C_s	M	−8392.4962	C_{2v}		−9551.6256	C_{2v}	
37	−34 302.6067	C_{3v}	c	−8646.8835	C_{3v}	c	−9836.6867	C_{2v}	
38	−35 419.9804	O_h	f	−8917.7056	O_h	f	−10 117.2454	O_h	f
39	−36 364.8587	C_{4v}	f	−9156.5715	C_{4v}	f	−10 389.6477	C_{4v}	f
40	−37 324.3708	C_s	M	−9397.0850	C_s		−10 661.9303	D_{4h}	f
41	−38 316.5698	C_s	c	−9643.6606	C_s	c	−10 934.9766	C_s	
42	−39 301.6696	C_s	M	−9892.1913	C_s		−11 211.5400	C_s	
43	−40 341.8543	C_s	M	−10 140.5484	C_s		−11 490.3063	C_{2v}	d4
44	−41 310.9157	C_1	M	−10 391.3783	C_2		−11 767.0685	C_s	
45	−42 345.0912	C_s	d4	−10 642.7040	C_s	d4	−12 039.6977	C_1	
46	−43 436.2827	C_{2v}	M	−10 900.4123	C_{2v}	M	−12 318.3028	C_3	
47	−44 405.1884	C_1	M	−11 145.6538	C_1	M	−12 595.3291	C_{2v}	d4
48	−45 470.1069	C_{2v}	d4	−11 411.4049	C_{2v}	d4	−12 875.3949	C_1	
49	−46 521.2131	C_{3v}	M	−11 662.0840	C_{3v}	M	−13 150.8235	D_{5h}	d4
50	−47 518.6719	D_{3h}	c	−11 920.7434	D_{3h}	c	−13 433.4182	D_{3h}	c
51	−48 522.4267	C_{2v}	M	−12 160.5960	C_s	c	−13 705.6730	C_s	c
52	−49 616.1377	C_{3v}	M	−12 424.6351	C_{2v}	M	−13 986.6288	C_{2v}	
53	−50 706.4665	C_{2v}	M	−12 689.2438	C_{2v}	M	−14 261.3449	C_{3v}	
54	−51 796.0777	C_{5v}	M	−12 953.6990	C_{5v}	M	−14 542.6311	C_{2v}	f
55	−52 884.6806	I_h	M	−13 217.8963	I_h	M	−14 814.5225	C_1	f
56	−53 756.6516	C_{3v}	M	−13 445.8961	C_s		−15 098.5064	D_{2h}	f
57	−54 700.1733	C_s	aM	−13 684.1489	C_s		−15 377.3233	C_{2v}	d5
58	−55 753.8515	C_{3v}	aM	−13 943.4015	D_{3h}	d4	−15 647.9269	C_s	d5
59	−56 751.4572	T_d	c	−14 202.4032	T_d	c	−15 928.8952	C_{2v}	d5
60	−57 763.6760	C_s	aM	−14 445.8412	C_{2v}	d5	−16 206.2020	C_{2v}	d5
61	−58 809.0448	C_{2v}	aM	−14 703.3954	C_{3v}	c	−16 495.9638	C_{3v}	c
62	−59 765.2180	C_{2v}	aM	−14 951.2644	C_s		−16 768.1774	C_s	c
63	−60 822.3826	C_s	d5	−15 213.6371	C_{2v}		−17 048.9913	C_s	c
64	−61 925.6244	C_{2v}	d5	−15 480.8530	C_{2v}	d5	−17 336.8555	C_{2v}	d5
65	−62 903.7387	C_{2v}	d5	−15 724.8185	C_{2v}	d5	−17 610.0214	C_{2v}	d5
66	−63 959.3105	C_s	d5	−15 985.0232	C_s	d5	−17 890.9860	C_s	d5
67	−65 011.2767	C_{2v}	d5	−16 244.0284	C_{2v}	d5	−18 169.0668	C_{2v}	d5
68	−65 980.5983	C_{3v}	c	−16 490.5019	C_{3v}	c	−18 448.5177	C_{3v}	c
69	−67 020.4042	C_1	d5	−16 744.2741	C_{2v}	d5	−18 725.1157	C_1	d5
70	−68 114.9462	C_s	d5	−17 012.0775	C_s	d5	−19 008.8021	C_s	d5
71	−69 216.6518	C_{2v}	d5	−17 279.8708	C_{2v}	d5	−19 300.7255	C_{2v}	d5
72	−70 171.4663	C_1	d5	−17 520.4788	C_1	d5	−19 573.7638	C_s	d5
73	−71 225.8547	C_{2v}	d5	−17 779.2971	C_s	d5	−19 855.7668	C_s	d5
74	−72 318.7243	C_{5v}	d5	−18 047.0929	C_{5v}	d5	−20 138.8921	C_{5v}	d5
75	−73 421.0521	D_{5h}	d5	−18 315.1577	D_{5h}	d5	−20 431.3452	D_{5h}	d5
76	−74 375.6975	C_s	d5	−18 554.6196	C_{2v}	d5	−20 704.2050	C_{2v}	d5
77	−75 430.9852	C_{2v}	d5	−18 814.0659	C_{2v}	d5	−20 978.9269	C_{2v}	d5
78	−76 385.4318	C_1	d5	−19 054.3977	C_s	d5	−21 252.2801	C_s	d5
79	−77 456.0255	D_{3h}	c	−19 321.0094	D_{3h}	c	−21 547.5979	O_h	f
80	−78 414.6271	C_s	c	−19 560.8966	C_s	c	−21 819.9952	C_{4v}	f

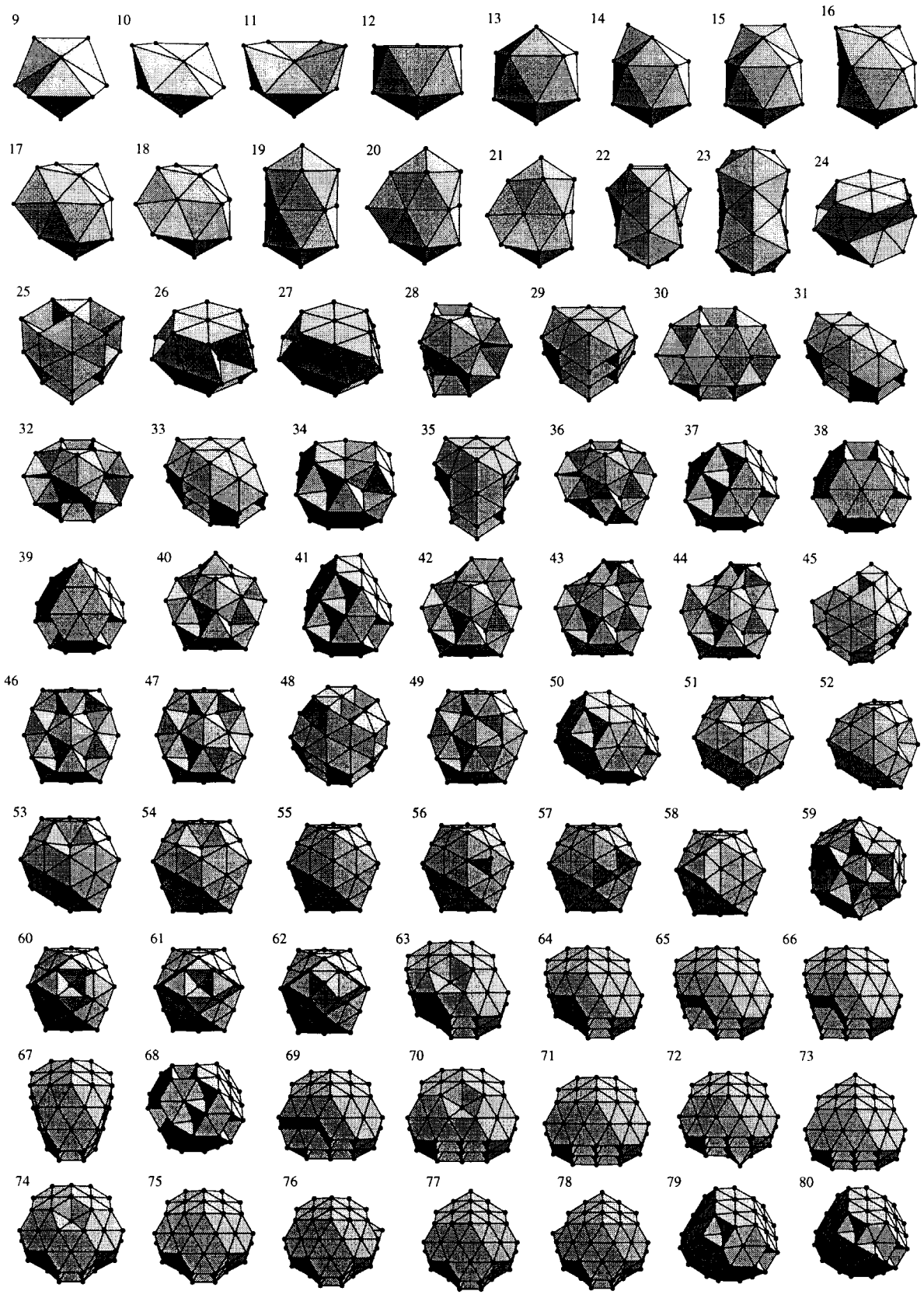

Fig. 2 Structures of the global minima for SC 12–6 clusters

peratures or number of steps for the MC runs in the present work.

It is interesting to note that 91% of the 12–6 global minima are also global minima for Morse clusters, 63% of the 9–6 and 39% of the 10–8. The decreasing percentages reflect the relative propensity of these potentials to give clusters with ordered structures of icosahedral, decahedral or close-packed morphologies. These values also confirm our suggestion that the database of Morse global minima would be useful in providing candidate structures for studies with more sophisticated potentials.[16] Furthermore, the results imply that some of the factors determining which isomer of a particular morphology is most stable are the same for a simple pair potential and for the more realistic many-body potentials used here.

Indeed, virtually all the Sutton–Chen clusters that have an ordered icosahedral, decahedral or close-packed structure were found in the reoptimization of the larger Morse database (global minima and low-lying isomers), where the primary structural principle is the maximization of the number of nearest neighbours.

The results presented here match or better all previously published results for Sutton–Chen clusters. We seem to have found the same structures as Nayak *et al.*, who examined all 9–6 clusters with $N \leqslant 23$, though we cannot be sure of this because no energies were given in that paper.[35] Uppenbrink and Wales studied a selection of 12–6 and 10–8 clusters in terms of their thermodynamics and dynamics.[36] They attempted to find the global minima by performing regular minimizations from molecular dynamics trajectories. It is interesting to note that for the two largest sizes they considered ($N = 40$ and 55), the true global minimum was found in only one of the four cases.

Silver and rhodium (SC 12–6) clusters

The structures of the 12–6 global minima are illustrated in Fig. 2 and the energies are plotted in Fig. 3(*a*). A function of the form $a + bN^{1/3} + cN^{2/3} + dN$, which has been fitted to the energy, is subtracted to emphasize the size dependence. In Fig. 3(*b*) $\Delta_2E(N) = E(N + 1) + E(N - 1) - 2E(N)$ is also illustrated; Δ_2E measures the stability of a structure with respect to neighbouring sizes. Peaks in Δ_2E have been found to correlate well with the magic numbers observed in mass spectra,[37] that is the sizes at which clusters are particularly abundant.

From Fig. 3(*a*) it can be seen that the most stable structures occur at sizes corresponding to complete Mackay icosahedra[11] ($N = 13$ and 55). This result was expected; it has been estimated from comparisons of stable sequences of clusters that the Mackay icosahedra are lowest in energy for up to a few thousand atoms for this potential.[38] This result also agrees with an *ab initio* study of silver clusters where, at the few sizes considered, icosahedra were always lower in energy than fcc structures.[13] The predominance of icosahedral morphologies might also be expected from the behaviour of the

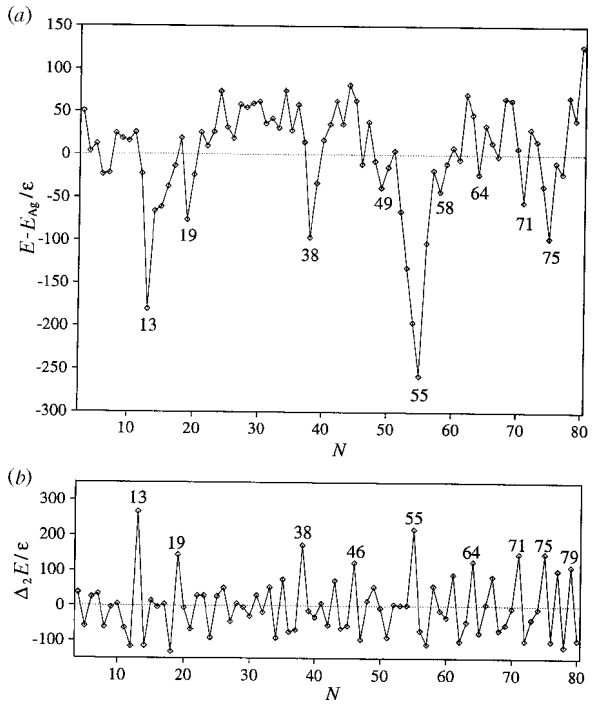

Fig. 3 (*a*) Energies and (*b*) Δ_2E for SC 12–6 clusters. In (*a*) the energy zero is $E_{Ag} = 940.6021 - 994.8068N^{1/3} + 1126.5506N^{2/3} - 1201.3951N$, where the coefficients have been chosen to give the best fit to the energies

Lennard-Jones potential to which the current functional form bears some resemblance. For Lennard-Jones clusters there are only four non-icosahedral global minima in the range $13 \leqslant N \leqslant 80$.[14] However, for the SC 12–6 potential there are only 30 icosahedral global minima in this size range; at sizes between the complete Mackay icosahedra other types of structure become lower in energy. Clearly the many-body part of the potential is important in determining the most stable structure.

Initially the growth sequence is similar to that of Lennard-Jones clusters. From $N = 7$ to 13 growth occurs by capping the seven-atom pentagonal bipyramid and leads to the 13-atom icosahedron. The one exception is the eight-atom cluster for which a deltahedral dodecahedron is lower in energy than the capped pentagonal bipyramid. Growth on a Mackay icosahedron can occur in two ways. In the first, the anti-Mackay overlayer, the atoms are added in sites that are hexagonal close-packed (hcp) with respect to the 20 tetrahedra that make up the icosahedron; for example, for the 13-atom icosahedron atoms are added to the centres of the faces and to the vertices. In the second, the Mackay overlayer, the atoms are added in sites that are fcc with respect to the underlying tetrahedra, which leads to the next Mackay icosahedron. From $N = 14$ to 21 growth occurs in the anti-Mackay layer, passing through the stable 19-atom double icosahedron (Fig. 3). However, above this size there are many types of competing structure and the global minimum changes frequently with size. Not until $N = 51$ are the structures again uniformly icosahedral, leading to the complete Mackay icosahedron at 55 atoms; Mackay icosahedra with one and two faces missing do give rise to the shallow minima in the energy plot at $N = 46$ and 49 [Fig. 3(*a*)].

Some of the global minima exhibit decahedral and close-packed morphologies. In Table 1 the close-packed clusters have been divided into those that are hcp, those that are fcc and those that involve a mixture of stacking sequences and twin planes. The most stable cluster in this intermediate size range is the 38-atom truncated octahedron [Fig. 3(*a*)]. The stability of this structure has recently been recognized in both theoretical[15,16] and experimental[9] work. Its shape is close to the ideal Wulff polyhedron and it is the only fcc structure that is the global minimum for the Lennard-Jones potential in this size range.[15]

For some of the decahedral clusters the (pseudo)-fivefold axis is not always obvious; it is obscured by overlayers on the {111} faces surrounding the axis at $N = 25$, 30, 45 and 48 for this potential (and at $N = 45$, 48, 58 for the 9–6 potential). Also, two global minima ($N = 22$ and 23) do not belong to any of the ordered morphologies. The 23-atom structure is based on two distorted face-sharing icosahedra and has been found before for Morse clusters;[16] the 22-atom structure is similar.

Growth on the 55-atom Mackay icosahedron again begins in the anti-Mackay overlayer; this leads to the weak minima in the energy plot of Fig. 3(*a*) at $N = 58$ and 61, which correspond to complete overlayers on one or two faces of the icosahedron. However, decahedral structures soon become lower in energy. From $N = 63$ a growth sequence begins, which leads to the 75-atom Marks decahedron. The latter structure's stability is clear from Fig. 3.

Unfortunately, it is difficult to make any critical assessment of the performance and reliability of the SC 12–6 potential because there has been little theoretical or experimental work on the structure of silver or rhodium clusters in the size range we consider here.

Nickel and copper (SC 9–6) clusters

The 9–6 global minima are illustrated in Fig. 4 and the size dependence of the energies and Δ_2E are given in Fig. 5. The

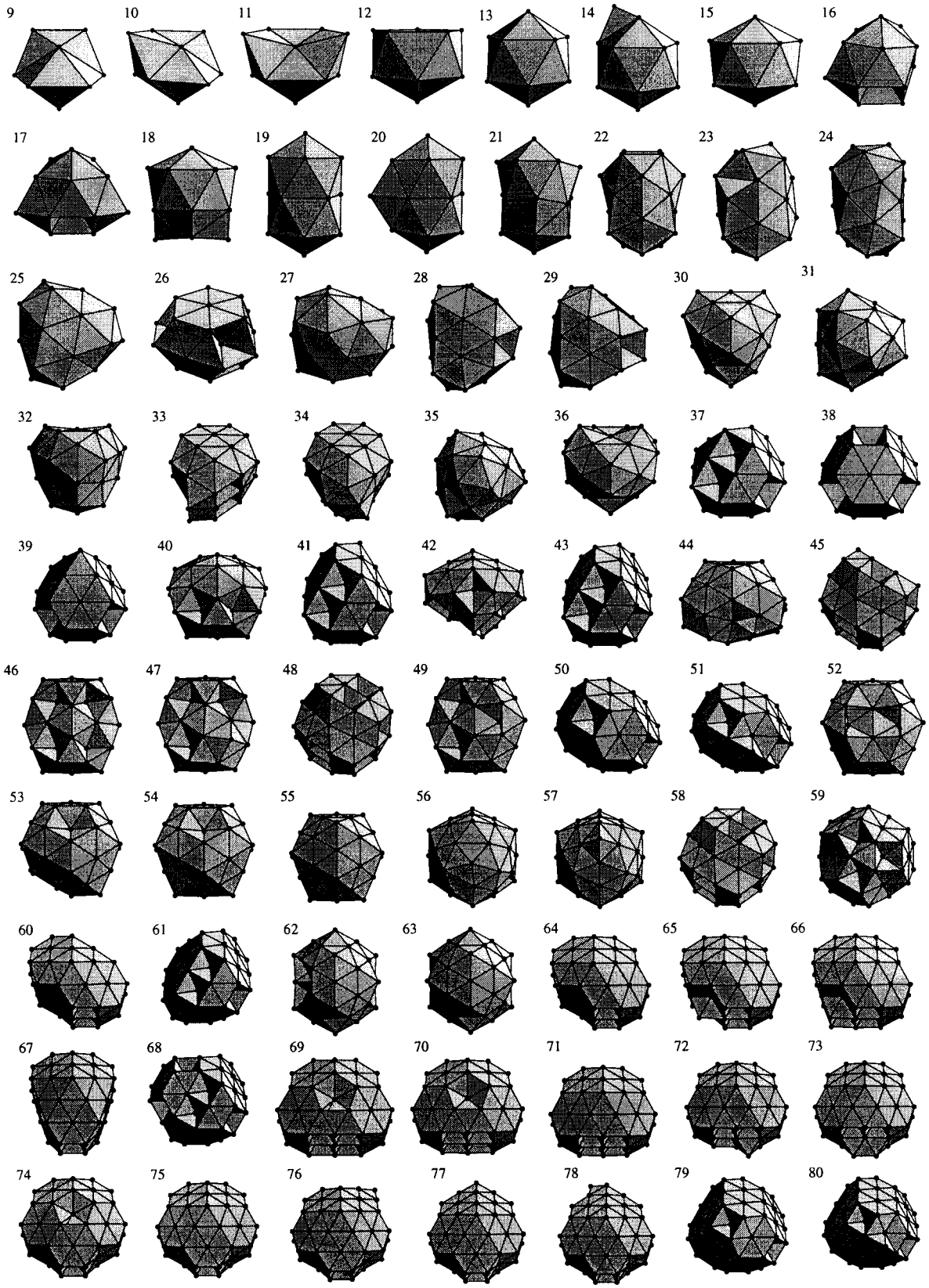

Fig. 4 Structures of the global minima for SC 9–6 clusters

latter figure is very similar to that found for the 12–6 clusters (Fig. 3): Mackay icosahedra are again most prominent, followed by the truncated octahedron and the Marks decahedron. However, the differences between the depths of the icosahedral ($N = 13$, 55) and non-icosahedral ($N = 38$, 75) minima in the energy plot in Fig. 5(*a*) are reduced compared to Fig. 3(*a*). This reflects a slight stabilization of the fcc and decahedral structures with respect to the icosahedra. Moreover, there are no subsidiary minima in the energy plot due to icosahedral structures at $N = 19$, 46 and 49. In total there are only 11 icosahedral minima in the size range $13 \leqslant N \leqslant 80$.

Two additional close-packed structures at $N = 50$ and 59 become more prominent in Fig. 5. The 50-atom cluster has D_{3h} point group symmetry and has a twin plane passing

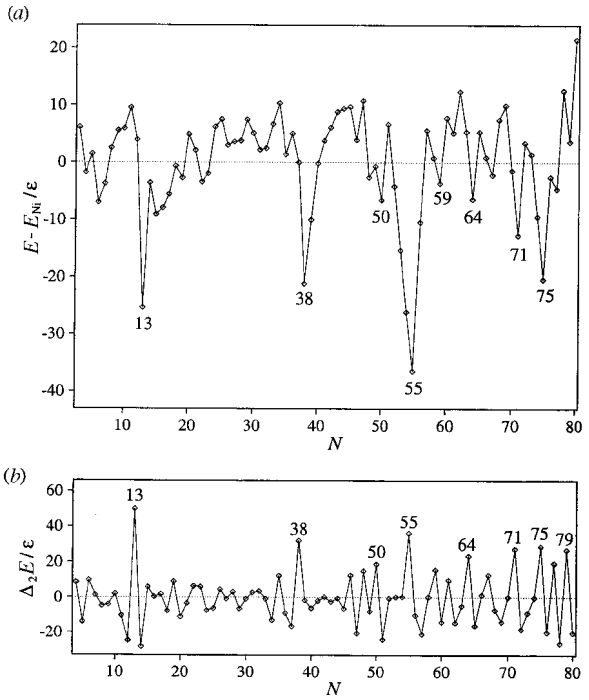

Fig. 5 (*a*) Energies and (*b*) $\Delta_2 E$ for SC 9–6 clusters. In (*a*) the energy zero is $E_{Ni} = 271.8994 - 292.8873N^{1/3} + 260.6812N^{2/3} - 292.9018N$, where the coefficients have been chosen to give the best fit to the energies

through the centre; each half of the cluster on either side of this twin plane is a fragment of the 38-atom truncated octahedron. An analogous structure is the global minimum for $N = 79$. The 59-atom cluster is based on the 31-atom truncated tetrahedron with the four sides covered by seven-atom hexagonal overlayers. Both are global minima for Morse clusters.[16]

Probably the biggest difference from the 12–6 clusters is the large number of global minima in the range $N = 16$ to 44 that do not belong to any of the ordered morphologies. There are 25 such structures. The central atom of the 15-atom cluster is 14-coordinate. This structure is one of the Frank–Kasper coordination polyhedra[39,40] and is the global minimum for a long-ranged Morse potential.[16] A single negative disclination[41] runs through this cluster. The 16- and 17-atom structures are based on the 13-atom Ino decahedron with three and four of the square faces capped, respectively. However, the structures distort so that two caps approach to form a nearest-neighbour contact. They are related to the undistorted decahedra by a single diamond-square-diamond rearrangement.[42] The structures for $N = 21$ to 24 are similar to the 23-atom 12–6 global minimum, which is made up of two distorted face-sharing icosahedra. The 25-atom cluster is based on a C_{3v} fcc structure, but with the triangular face twisted to remove {100} facets. The 34-atom cluster resembles the decahedral 33-atom structure; however, the additional atom causes one part of the cluster to distort. The 40-atom global minimum is based on an icosahedral structure with a Mackay overlayer (as for 12–6). However, a low-coordination-number atom in that structure has been absorbed into the surface. Similarly, the 56- and 57-atom clusters are based on the Mackay icosahedron. The first adatom adsorbs into the surface layer with an accompanying distortion, rather than occupying a three-coordinate site on the surface. The second adatom then occupies a four-coordinate site on the resulting distorted surface. Similar avoidance of structures with atoms of low coordination number has been seen in calculations for nickel by Wetzel and DePristo.[43] The 62- and 63-atom structures are based on the 52-atom global minimum, which is a Mackay icosahedron with an edge removed. Two triangular faces are added over this missing edge.

How can these relatively disordered structures become global minima and why do they disappear at larger sizes? Probably because most of these geometries are more spherical, have a larger number of nearest-neighbour contacts and involve fewer low coordination-number atoms than structures based on one of the ordered morphologies. However, this advantage is counterbalanced by the introduction of considerable strain. As the energetic penalty for the strain scales with the volume,[15,44] it can only be accommodated at smaller sizes.

For the elements described by this potential there is a wealth of theoretical and experimental work to compare with our results, mainly due to the pioneering efforts of Riley and coworkers on nickel clusters. First we compare our results to other theoretical studies, which use different descriptions of the interactions. Of these studies the most comprehensive is that of DePristo and coworkers who used the corrected effective medium theory to look at all clusters up to $N = 55$.[43,45] They found that at $N = 13$ and 55 the favoured geometries were icosahedral. However, for many of the intermediate sizes, especially when the icosahedral structure at that size would involve a low-coordination-number surface atom, the global minima did not belong to any of the ordered morphologies. At some sizes these disordered structures appear to be the same as found in this study, for example $N = 15$, 18 and 25. DePristo *et al.*[43,45] did not identify any of the global minima as close-packed or decahedral, although it seems that their 38-atom structure is in fact a distorted truncated octahedron.[9]

Using a tight-binding model Lathiotakis *et al.* studied a selection of clusters with up to 55 atoms.[46] Of the structures they considered, they found that Mackay icosahedra were lowest in energy at $N = 13$ and 55, but at some intermediate sizes fcc structures were lower in energy than icosahedral clusters. However, only a few structures were considered at each size and these may not include the global minima.

Montejano *et al.* used an embedded-atom potential to compare the energies of icosahedral structures, in particular to locate the size at which the transition from an anti-Mackay to a Mackay overlayer occurred.[47] However, these results are not relevant to many sizes since theory and experiment suggest that other non-icosahedral structures are lowest in energy.

Hu *et al.* attempted to model the interatomic interactions using a long-ranged Morse potential.[48] As expected for a Morse potential with a range parameter[16] $\rho_0 = 3.54$ they observed icosahedral structures with an anti-Mackay overlayer up to $N = 40$. However, a Morse potential is probably not a good approximation to the real nickel potential; therefore these results differ from experimental and other theoretical studies.

Most recently, Curotto *et al.* employed a tight-binding potential and performed systematic searches for global minima up to 14 atoms.[49] Their lowest energy structure for Ni_{13} is not icosahedral and they comment that the 'growth pattern is nontrivial'. They suggest that the global minima show a preference for more uniform coordination of every atom rather than maximization of the total number of nearest-neighbour contacts.

Icosahedral structure was first identified for nickel clusters by looking at the size dependence of the chemical reactivity with various probe molecules.[50–52] Features were found at sizes corresponding to complete Mackay icosahedra and also for icosahedral structures with stable surface overlayers. Subsequently, icosahedral magic numbers have also been seen in mass spectra for $50 \leqslant N \leqslant 800$.[53]

The most detailed structural information has come from work using nitrogen probe molecules.[6–10] This technique has enabled assignments to be made for the majority of clusters in

Table 2 Coordination number analysis and estimated number of N_2 binding sites for SC 9–6 clusters. The number of binding sites has been calculated using the rules given in the text. The values in parentheses are appropriate if nine-coordinate binding sites are included. For 38 atoms and above there is no evidence of this type of binding and the alternative values have been omitted. The nearest-neighbour criterion used is 0.8*a*

		Coordination number							
N	N_2 binding sites	3	4	5	6	7	8	9	⩾10
4	8	4							
5	10	2	3						
6	12		6						
7	12		5	2					
8	12		4	4					
9	13		4	2	2		1		
10	12(13)		3	3	3			1	
11	12		2	4	4				1
12	11			5	6				1
13	12				12				1
14	14				9	3			1
15	14				12	2			1
16	16		1	2	12				1
17	18		2		10	4			1
18	19		2		8	7			1
19	17				12		5		2
20	19		1		10	2	5		2
21	19			1	12	1	5		2
22	20			3	11	4	2		2
23	21				14	6	1		2
24	22			2	10	6	4		2
25	21(22)				12	3	6	1	3
26	21(24)			6	12		3	2	3
27	24				13	4	7		3
28	25				13	7	5		3
29	26			2	12	6	6		3
30	26			1	13	4	8		4
31	24(27)			3	12	3	6	3	4
32	24(28)				12			4	4
33	26(26)			4	14	2	6	2	5
34	26(30)			2	14	6	4	4	4
35	30				12	6	8		5
36	30				16	6	8		6
37	27(31)			3	18	3	3	4	6
38	24				24			8	6
39	26		1		20	4		8	6
40	33				14	6	13		7
41	29			3	18	4	4	5	7
42	35			2	18	1	14		7
43	29			3	18	4	4	7	7
44	35				14	10	11		9
45	32			2	19	5	6	3	10
46	35				16	2	17	2	9
47	36			1	16	2	17	2	9
48	35				22	2	11	2	11
49	36				15	3	18	3	10
50	30				24	6		8	12
51	32		1		22	7	1	8	12
52	39				14	4	21		13
53	40				10	10	20		13
54	41				11	5	25		13
55	42				12		30		13
56	43				10	11	22		13
57	45		1		9	9	25		13
58	39				24	6	9		19
59	36				24	12		4	19
60	41				22		13	4	15
61	36				24	6	6	12	13
62	46				15	3	28		16
63	46				16		32		17
64	40				22	8	10	6	18
65	42		1		22	6	12	6	18
66	42			2	20	7	13	6	18
67	44				22	6	16	6	17
68	39				24	9	6	13	16
69	41				20	18	3	8	18
70	42				21	13	8	8	19
71	43				22	8	13	8	20
72	43		1		21	8	12	10	20
73	41			2	20	9	10	11	21
74	41				21	15	5	10	23
75	42				22	10	10	10	23
76	44		1		18	14	10	10	23
77	44			2	18	12	12	10	23
78	46		1		20	10	14	10	23
79	39				24	12	3	18	22
80	41		1		22	13	4	18	22

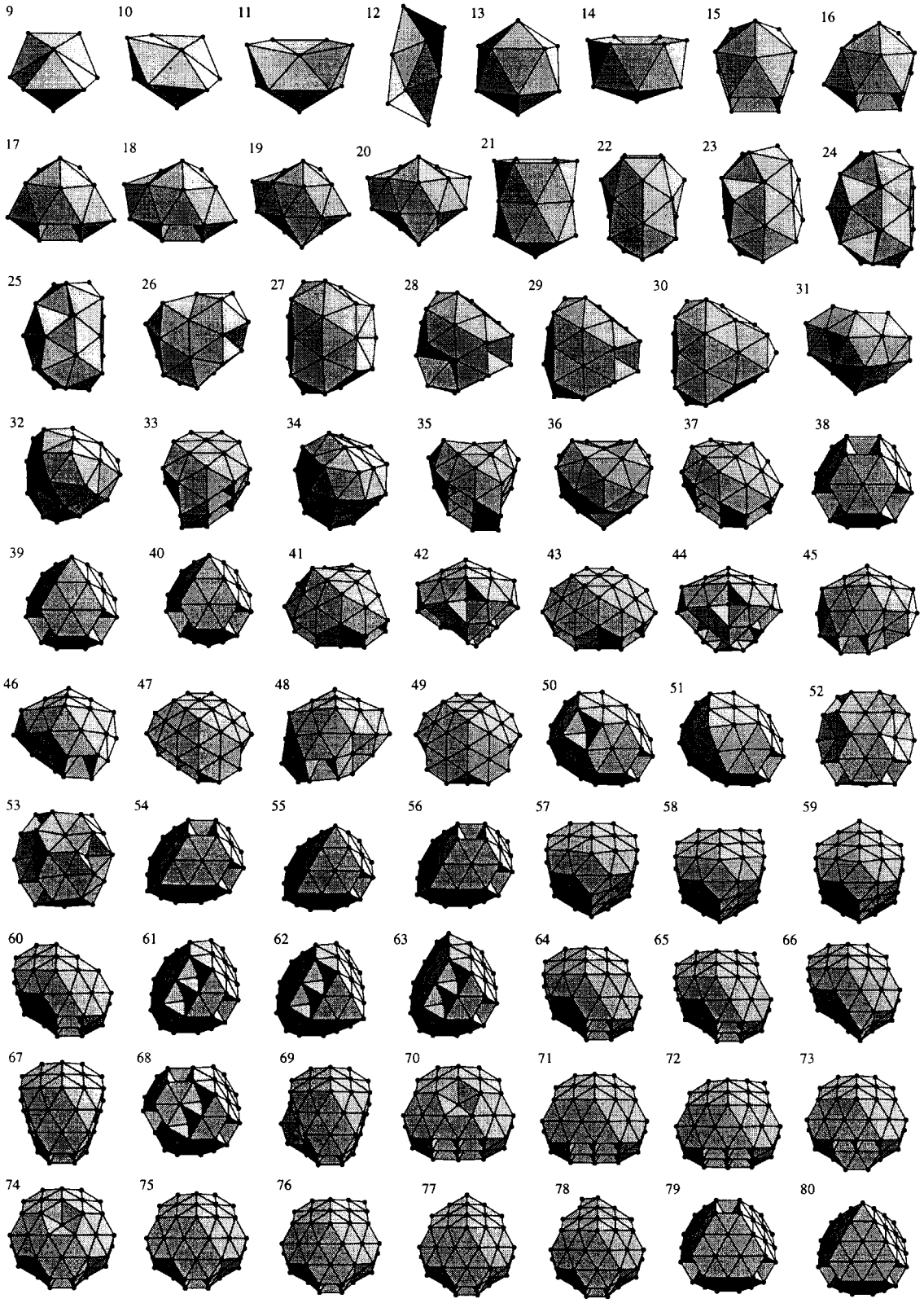

Fig. 6 Structures of the global minima for SC 10–8 clusters

the range $N \leqslant 28$, $49 \leqslant N \leqslant 71$ and at $N = 38$. However, in the intermediate size range, structural assignments based on these nitrogen experiments have not yet been published due to the difficulty in interpreting the experimental data.

In agreement with our work Parks *et al.* found that the structures at $N = 13$ and 55 are Mackay icosahedra,[6,7] whilst $N = 38$ is a truncated octahedron.[9] In the range $13 < N \leqslant 26$ the experiments with nitrogen indicate that most of the structures are formed by the addition of an anti-Mackay overlayer to the 13-atom icosahedron, from $N = 49$ to 55 the Mackay overlayer is completed, and then up to $N = 71$ an anti-Mackay overlayer grows on the 55-atom Mackay icosahedron. The reactivity of nickel clusters with ammonia, water,[51] hydrogen[52] and deuterium[54] also suggests that icosahedral structures persist above $N = 71$. These assignments differ from our 9–6 results in that the Sutton–Chen potential seems to underestimate the stability of icosahedral structures. However, non-icosahedral clusters do seem to occur in the range $29 \leqslant N \leqslant 48$, in agreement with the SC 9–6 potential. If disordered global minima are indeed observed in this size range

for real nickel clusters, this would help to explain the difficulties experienced by Riley and coworkers in assigning structures.

To further facilitate comparisons with experiment we have estimated the number of binding sites for nitrogen using the rules formulated by Parks *et al.*[6] These are: (1) N_2 binds directly to the nickel atoms; (2) a nickel atom with a coordination number of four or less binds two N_2 molecules; (3) nickel atoms with a coordination number of five to eight bind one N_2 molecule; (4) nickel atoms with a coordination number of nine bind N_2 molecules weakly or not at all and (5) nickel atoms with a coordination number of ten or more do not bind N_2. To clarify rule (4) it has been found that for smaller clusters N_2 can bind to a nine-coordinate atom, but for the larger clusters ($N > 49$) no evidence has been found for this type of binding. The number of binding sites and the coordination number analysis for the 9–6 global minima are given in Table 2. For the clusters with an ordered morphology the differentiation between nearest neighbours and next-nearest neighbours is clear. However, this differentiation becomes ambiguous for the disordered structures and so the coordination number analysis, and sometimes the number of N_2 binding sites, becomes dependent on the nearest-neighbour criterion that is used.

The magnetic moments of size-selected nickel clusters have been measured for all clusters up to $N = 200$.[4] For small N there is considerable variation of the magnetic moment with size. It was concluded that features at $N = 13$ and 55 indicate an icosahedral structure.[4] However, it is difficult to decipher the structural information that is contained in other features of the magnetic moment size dependence.

Much less structural information is available for copper clusters. Recent experiments suggest that icosahedra predominate up to $N \approx 2500$ atoms and above this fcc clusters are more prevalent.[55] Although that study encompasses clusters far larger than we consider here, our results are not inconsistent with this finding.

Gold and platinum (SC 10–8) clusters

The 10–8 global minima are illustrated in Fig. 6 and the size dependence of the energies and $\Delta_2 E$ are given in Fig. 7. The latter figure shows a very different pattern from that seen for the 12–6 or 9–6 clusters: there are no signatures due to icosahedral clusters. Although the 13-atom icosahedron is the global minimum, above this size there are no global minima with ordered icosahedral structures. Instead, Fig. 7(*a*) is dominated by features due to particularly stable close-packed and decahedral clusters. The 38-atom fcc truncated octahedron and the 75-atom Marks decahedron exhibit the deepest minima in Fig. 7(*a*). There are also minima in the energy plot at $N = 64$ and 71, due to incomplete Marks decahedra, and at $N = 50$, 61 and 79, due to close-packed clusters. The 50-atom global minimum is the 'twinned truncated octahedron' that is the global minimum for the SC 12–6 and 9–6 potentials. The 61-atom structure is a fragment of the 79-atom twinned truncated octahedron, which is the global minimum for the SC 12–6 and 9–6 potentials, and the 79-atom global minimum is a truncated octahedron. The 10–8 potential's greater preference for fcc structures, rather than close-packed structures involving twin planes, is illustrated by the fcc global minimum at $N = 79$. For $N = 54$ to 56 fcc structures are also lowest in energy and the 59-atom close-packed structure with T_d symmetry is not the global minimum, in contrast to the SC 12–6 and 9–6 potentials.

As for the 9–6 potential, between $N = 13$ and 55 there is a tendency to form structures that do not fit neatly into one of the ordered morphologies. In total there are 31 such structures compared to 25 for the SC 9–6 potential. The 14- and 21-atom structures are based on the SC 9–6 15-atom global

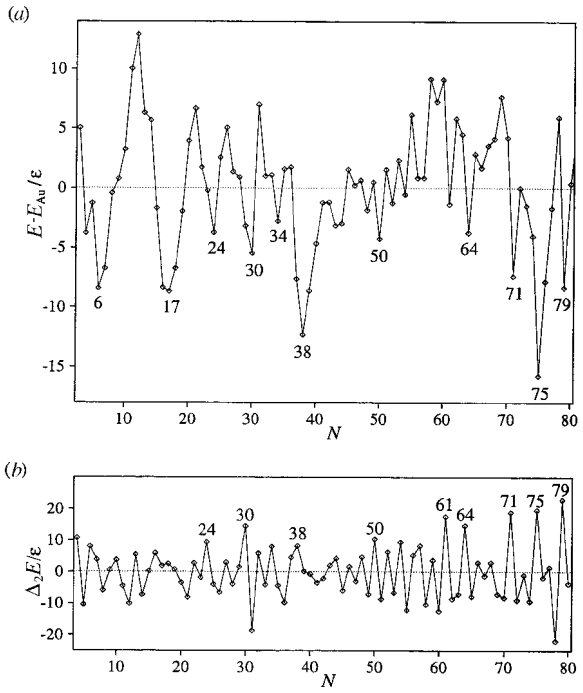

Fig. 7 (*a*) Energies and (*b*) $\Delta_2 E$ for SC 10–8 clusters. In (*a*) the energy zero is $E_{Au} = 277.5753 - 276.0472N^{1/3} + 192.0783N^{2/3} - 305.9338N$, where the coefficients have been chosen to give the best fit to the energies

minimum. The 14-atom cluster has one of the seven-coordinate vertices removed and the 21-atom structure is formed when six atoms are added to the faces surrounding a vertex, thus extending the negative disclination line.[16] The structures for $N = 15$ to 20, like the 15- and 16-atom SC 9–6 global minima, are based on distorted decahedra. Similar distorted decahedra are also observed at $N = 35$, 37 and 41.

The global minima for $N = 22$ to 30 are structurally related. The smaller clusters resemble the 23-atom D_{3h} SC 12–6 global minimum and the larger ones are related to a 30-atom structure that is made up of three interpenetrating D_{3h} units. Interestingly, the 24- and 30-atom structures produce minima in the energy plot in Fig. 7(*a*).

Many of the other disordered structures have, in part, the surface structure of an incomplete Mackay icosahedron, but are distorted in various ways, for example $N = 31$, 36, 42, 44, 46, 48, 52 and 53. The 53-atom structure is based on the Mackay icosahedron with three adjacent vertices removed, an atom added in the centre of this incomplete face and accompanying distortions. The 52-atom structure is then formed simply by the removal of one atom.

The main work to which our results can be compared is that of Whetten and coworkers for gold clusters passivated by alkylthiolates.[56–60] In these experiments the clusters selectively form specific sizes, which were isolated by fractional crystallization. Each fraction has a narrow size distribution. The clusters presumably form these specific sizes because of their stability. Furthermore, it is thought that the passivating surface layer does not perturb the structure significantly. If this is true then the observed structures reflect those of the free clusters.

Most of the cluster sizes formed were close to those expected for truncated octahedra.[56,61] For the smallest sizes detailed structural investigations were made by comparing experimental X-ray diffraction patterns with those calculated from structural models. This comparison led to the identification of the fractions with $N \approx 75$, 101 and 146 as Marks decahedra,[57,79] and those with $N \approx 225$, 459 as twinned truncated octahedra.[58] Recently, a fraction with $N \approx 38$ has also been

isolated; the diffraction patterns suggest that it is the fcc truncated octahedron.[60]

Our results for SC 10–8 agree very well with these experimental data. The two clusters observed experimentally for $N \leqslant 80$ are the two that we find to be the most stable, namely the 38-atom truncated octahedron and the 75-atom Marks decahedron.

Cleveland *et al.* have performed a number of theoretical studies to interpret the experimental results on passivated gold clusters.[58,59] They used an embedded-atom potential and looked at several sequences of structures. As in the present study, they found that truncated octahedra and Marks decahedra were most stable. They also found that introducing a twin plane into a truncated octahedron leads to an increase in energy; for example, for $N = 79$ the fcc O_h structure was slightly lower in energy than the twinned D_{3h} structure. This trend seems to disagree with the experimental results—at $N \approx 225$, 459 the diffraction patterns seem to suggest that the structure has a twin plane. Garzón and Posada-Amarillas also used the embedded-atom method to look at a 55-atom cluster.[62] They found that a disordered structure was lower in energy than the icosahedron.

We also note that at $N = 55$ the fcc cuboctahedron is not the global minimum; it actually lies 78.1ε above the fcc global minimum. In connection with this comment, it is interesting that a recent investigation of ligated 55-atom gold clusters, which were originally thought to be cuboctahedral,[63,64] seems to disprove this structural assignment.[65]

The only calculations for platinum that are relevant to our results are by Sachdev *et al.*[66,67] For clusters with up to 60 atoms they found that the lowest energy structures were disordered. In particular at $N = 55$ these structures were lower than the icosahedron and cuboctahedron. These results have some overlap with ours but it is not clear whether Sachdev *et al.* found the global minima for the larger sizes.

Conclusions

In this paper we have found the likely global minima for clusters with up to 80 atoms whose interactions are described by the SC family of potentials. These potentials can be used to model silver, rhodium, nickel, copper, gold and platinum clusters. The results are encouraging, in that the most stable structures generally appear to agree with experiment. For nickel clusters the 13- and 55-atom Mackay icosahedra, the 38-atom truncated octahedron and the 75-atom Marks decahedron are particularly stable. The former three clusters have been unambiguously identified in experimental studies of chemical reactivity using nitrogen as a probe molecule and it would be interesting to see if extensions of these experiments to $N = 75$ could identify the Marks decahedron. For gold clusters we find the 38-atom truncated octahedron and the 75-atom Marks decahedron to be particularly stable; Whetten and coworkers have isolated both these clusters passivated by alkylthiolates.[56–60]

Our results should also be useful in aiding structural assignments from experimental data on size-selected clusters and in providing candidate structures for calculations using more sophisticated descriptions of the interactions. For this reason the configurations of all global minima will be made available from the Cambridge Cluster Database.[32] However, it would be surprising if these empirical potentials could accurately reproduce all the intricacies of a particular cluster growth sequence. This is especially true when the energy differences between competing structures are small. In such cases the character of the global minimum will be particularly sensitive to the accuracy of the potential.

Given the uncertainties in any empirical potential, it is useful to compare the results obtained with different forms. Additional weight can then be given to those structural predictions that are common to a number of potentials, and where there is disagreement one can then look to more sophisticated calculations to provide a solution. For confident structural conclusions to be made from calculations using a higher level of theory one needs to compare the results from the reoptimization of a variety of potentially low energy structures. Global and low energy minima from a variety of potentials will help to provide such a database of candidate structures. For these reasons the results we describe here are complementary to previous work using different model potentials.

When comparing the structures described here to experiment, aside from possible inaccuracies in the potential, it should also be remembered that the global minimum is only rigorously the free energy global minimum at absolute zero. At finite temperature entropic effects may play a role in determining the most stable structure. These entropic effects are most likely to be influential when the energy gap between the global minimum and other low energy minima is small. For example, it has been shown that for a 38-atom Lennard–Jones cluster the structure changes from fcc to icosahedral as the temperature increases.[27] Similarly, for a 75-atom Morse cluster with a medium-ranged potential there is a transition from a Marks decahedron to icosahedral structures.[15] Both these transitions stem from the larger entropy of the icosahedra; there are many icosahedral minima that have energies just above the global minimum, whereas there is a large energy gap between the global minimum and the next lowest energy minimum with the same morphology. When energy differences between low energy structures are small experiments are likely to detect multiple isomers at relatively low temperatures.

Finally, the results presented here further illustrate the power of the 'basin-hopping' or Monte Carlo minimization global optimization algorithm.[26] This method has enabled us to locate global minima with some confidence for systems with up to 240 degrees of freedom, many of which exhibit a multiple funnel potential energy surface topography.

Acknowledgements

D.J.W. is grateful to the Royal Society for financial support. The work of the FOM Institute is part of the research program of 'Stichting Fundamenteel Onderzoek der Materie' (FOM) and is supported by NWO ('Nederlandse Organisatie voor Wetenschappelijk Onderzoek').

References

1 J. Farges, M. F. de Feraudy, B. Raoult and G. Torchet, *Adv. Chem. Phys.*, 1988, **70**, 45.
2 T. P. Martin, *Phys. Rep.*, 1996, **273**, 199.
3 S. J. Riley, in *Clusters of Atoms and Molecules II*, ed. H. Haberland, Springer Verlag, Berlin, 1994, p. 221.
4 S. E. Apsel, J. W. Emmert, J. Deng and L. A. Bloomfield, *Phys. Rev. Lett.*, 1996, **76**, 1441.
5 S. Kakar, O. Björneholm, J. Weigelt, A. R. B. de Castro, L. Tröger, R. Frahm, T. Möller, A. Knop and E. Rühl, *Phys. Rev. Lett.*, 1997, **78**, 1675.
6 E. K. Parks, L. Zhu, J. Ho and S. J. Riley, *J. Chem. Phys.*, 1994, **100**, 7206.
7 E. K. Parks and S. J. Riley, *Z. Phys. D*, 1995, **33**, 59.
8 E. K. Parks, L. Zhu, J. Ho and S. J. Riley, *J. Chem. Phys.*, 1995, **102**, 7377.
9 E. K. Parks, G. C. Niemann, K. P. Kerns and S. J. Riley, *J. Chem. Phys.*, 1997, **107**, 1861.
10 E. K. Parks, G. C. Niemann, K. P. Kerns and S. J. Riley, *J. Chem. Phys.*, 1998, **108**, 3731.
11 A. L. Mackay, *Acta Crystallogr.*, 1962, **15**, 916.
12 O. D. Häberlan, S.-C. Chung, M. Stener and N. Rösch, *J. Chem. Phys.*, 1997, **106**, 5189.
13 D. R. Jennison, P. A. Schultz and M. P. Sears, *J. Chem. Phys.*, 1997, **106**, 1856.
14 D. J. Wales and J. P. K. Doye, *J. Phys. Chem. A*, 1997, **101**, 5111.

15 J. P. K. Doye, D. J. Wales and R. S. Berry, *J. Chem. Phys.*, 1995, **103**, 4234.
16 J. P. K. Doye and D. J. Wales, *J. Chem. Soc., Faraday Trans.*, 1997, **93**, 4233.
17 L. D. Marks, *Philos. Mag. A*, 1984, **49**, 81.
18 L. D. Marks, *Rep. Prog. Phys.*, 1994, **57**, 603.
19 A. P. Sutton and J. Chen, *Philos. Mag. Lett.*, 1990, **61**, 139.
20 R. M. Lynden-Bell, *Surf. Sci.*, 1991, **259**, 129.
21 B. D. Todd and R. M. Lynden-Bell, *Surf. Sci.*, 1993, **281**, 191.
22 R. L. Blumberg, R. M. Lynden-Bell and W. M. Gelbart, *J. Chem. Phys.*, 1993, **98**, 9808.
23 R. M. Lynden-Bell, J. S. Van Duijneveldt and D. Frenkel, *Mol. Phys.*, 1993, **80**, 801.
24 K. D. Hammonds, *Mol. Phys.*, 1994, **81**, 227.
25 R. M. Lynden-Bell, *J. Phys.: Condens. Matter*, 1995, **7**, 4603.
26 Z. Li and H. A. Scheraga, *Proc. Natl. Acad. Sci. USA*, 1987, **84**, 6611.
27 J. P. K. Doye and D. J. Wales, *Phys. Rev. Lett.*, 1998, **80**, 1357.
28 F. H. Stillinger and T. A. Weber, *J. Stat. Phys.* 1988, **52**, 1429.
29 C. Baysal and H. Meirovitch, *J. Chem. Phys.*, 1996, **105**, 7868.
30 P. Derreumaux, *J. Chem. Phys.*, 1977, **106**, 5260.
31 P. Derreumaux, *J. Chem. Phys.*, 1997, **107**, 1941.
32 D. J. Wales, J. P. K. Doye, A. Dullweber and F. Y. Naumkin, The Cambridge Cluster Database, URL < http://brian.ch.cam.ac.uk/CCD.html >, 1998.
33 J. P. K. Doye and D. J. Wales, *Chem. Phys. Lett.*, 1995, **247**, 339.
34 J. P. K. Doye and D. J. Wales, *J. Chem. Phys.*, 1996 **105**, 8428.
35 S. K. Nayak, S. N. Khanna, B. K. Rao and P. Jena, *J. Phys. Chem. A*, 1997, **101**, 1072.
36 J. Uppenbrink and D. J. Wales, *J. Chem. Phys.*, 1993, **98**, 5720.
37 K. Clemenger, *Phys. Rev. B*, 1985, **32**, 1359.
38 J. Uppenbrink and D. J. Wales, *J. Chem. Phys.*, 1992, **96**, 8520.
39 F. C. Frank and J. S. Kasper, *Acta Crystallogr.*, 1958, **11**, 184.
40 F. C. Frank and J. S. Kasper, *Acta Crystallogr.*, 1959, **12**, 483.
41 D. R. Nelson and F. Spaepen, *Solid State Phys.*, 1989, **42**, 1.
42 W. N. Lipscomb, *Science*, 1966, **153**, 373.
43 T. L. Wetzel and A. E. DePristo, *J. Chem. Phys.*, 1996, **105**, 573.
44 D. J. Wales and J. P. K. Doye, in *Large Clusters of Atoms and Molecules*, ed. T. P. Martin, NATO ASI Series, Kluwer Academic, Dordrecht, 1996, vol. E313, pp. 241–279.
45 M. S. Stave and A. E. DePristo, *J. Chem. Phys.*, 1992, **97**, 3386.
46 N. N. Lathiotakis, A. N. Andriotis, M. Menon and J. Connolly, *J. Chem. Phys.*, 1996, **104**, 992.
47 J. M. Montejano-Carrizales, M. P. Iniguez, J. A. Alonso and M. J. Lopez, *Phys. Rev. B*, 1996, **54**, 5961.
48 W. Hu, L. Mei and H. Li, *Solid State Commun.*, 1996, **100**, 129.
49 D. L. F. E. Curotto, A. Matro and J. D. Doll, *J. Chem. Phys.*, 1998, **108**, 729.
50 B. J. Winter, T. D. Klots, E. K. Parks and S. J. Riley, *Z. Phys. D.*, 1991, **19**, 375.
51 E. K. Parks, B. J. Winter, T. D. Klots and S. J. Riley, *J. Chem. Phys.*, 1991, **94**, 1882.
52 T. D. Klots, B. J. Winter, E. K. Parks and S. J. Riley, *J. Chem. Phys.*, 1991, **95**, 8919.
53 M. Pellarin, B. Baguenard, J. L. Vialle, J. Lermé, M. Broyer, J. Miller and A. Perez, *Chem. Phys. Lett.*, 1994, **217**, 349.
54 E. K. Parks, G. C. Nieman and S. J. Riley, *Surf. Sci.*, 1996, **355**, 127.
55 D. Reinhard, B. D. Hall, S. Valkealahti and R. Monot, *Phys. Rev. Lett.*, 1997, **79**, 1459.
56 R. L. Whetten, J. T. Khoury, M. M. Alvarez, S. Murty, I. Vezmar, Z. L. Wang, P. W. Stephens, C. L. Cleveland, W. D. Luedtke and U. Landman, *Adv. Mater.*, 1996, **8**, 428.
57 M. M. Alvarez, J. T. Khoury, T. G. Schaaff, M. Shafigullin, I. Vezmar and R. L. Whetten, *Chem. Phys. Lett.*, 1997, **266**, 91.
58 C. L. Cleveland, U. Landman, M. N. Shafgullin, P. W. Stephens and R. L. Whetten, *Z. Phys. D.*, 1997, **40**, 503.
59 C. L. Cleveland, U. Landman, T. G. Schaaff, M. N. Shafgullin, P. W. Stephens and R. L. Whetten, Phys. Rev. Lett., 1997, **79**, 1873.
60 T. G. Schaaff, M. Shafigullin, J. T. Khoury, I. Vezmar, R. L. Whetten, W. G. Cullen, P. N. First, C. Guttiérez-Wing, J. Ascensio and M. J. Jose-Yacamán, *J. Phys. Chem. B*, 1997, **101**, 7885.
61 R. P. Andres, J. D. Bielefeld, J. I. Henderson, D. B. Janes, V. R. Kolagunta, C. P. Kubiak, W. J. Mahoney and R. G. Osifchin, *Science*, 1996, **273**, 1690.
62 I. L. Garzón and A. Posada-Amarillas, *Phys. Rev. B*, 1996, **54**, 11796.
63 G. Schmid, R. Pfeil, R. Boese, F. Bandermann, S. Meyer, G. H. M. Calis and J. W. A. van der Velden, *Chem. Ber.*, 1981, **114**, 3634.
64 L. R. Wallenberg, J. O. Bovin and G. Schmid, *Surf. Sci.*, 1985, **156**, 256.
65 H. C. D. H. Rapoport, W. Vogel and R. Schlögl, *J. Phys. Chem. B*, 1997, **101**, 4175.
66 A. Sachdev, R. I. Masel and J. B. Adams, *Catal. Lett.*, 1992, **15**, 57.
67 A. Sachdev, R. I. Masel and J. B. Adams, *Z. Phys. D*, 1993, **26**, 310.

Received in Montpellier, France, 10*th November* 1997;
Paper 7/09249K